

Helical Majorana fermions in $d_{x^2-y^2} + id_{xy}$ -wave topological superconductivity of doped correlated quantum spin Hall insulators

Shih-Jye Sun¹, Chung-Hou Chung^{2,3}, Yung-Yeh Chang², Wei-Feng Tsai⁴, and Fu-Chun Zhang^{5,6}

¹*Department of Applied Physics, National University of Kaohsiung, Kaohsiung, Taiwan, R.O.C.*

²*Electrophysics Department, National Chiao-Tung University, HsinChu, Taiwan, 300, R.O.C.*

³*Physics Division, National Center for Theoretical Sciences, HsinChu, Taiwan, 300 R.O.C.*

⁴*Department of Physics, National Sun Yat-Sen University, Kaohsiung, Taiwan, R.O.C.*

⁵*Department of Physics, Zhejiang University, Hangzhou, China*

⁶*Collaborative Innovation Center of Advanced Microstructures, Nanjing, China*

(Dated: August 31, 2021)

Large Hubbard U limit of the Kane-Mele model on a zigzag ribbon of honeycomb lattice near half-filling is studied via a renormalized mean-field theory. The ground state exhibits time-reversal symmetry (TRS) breaking $d_{x^2-y^2} + id_{xy}$ -wave superconductivity. At large spin-orbit coupling, the Z_2 phase with non-trivial spin Chern number in the pure Kane-Mele model is persistent into the TRS broken state (called “spin-Chern phase”), and has two pairs of counter-propagating helical Majorana modes at the edges. As the spin-orbit coupling is reduced, the system undergoes a topological quantum phase transition from the spin-Chern to chiral superconducting states. Possible relevance of our results to adatom-doped graphene and iridate compounds is discussed.

PACS numbers: 72.15.Qm, 7.23.-b, 03.65.Yz

Introduction. Searching for topological states of quantum matters constitutes one of the central and fundamental issues in condensed matter systems. The growing interest in topological insulators (TIs), which support gapless edge (or surface) states protected by time-reversal symmetry (TRS) while the bulk remains insulating [1, 2], is one prime example. Of particular interest are topological superconductors which support gapless self-conjugate, charge-neutral fermionic quasi-particle excitations [3]. These excitations which reflect non-trivial topological bulk properties are localized at the edges, known as Majorana fermions (MFs).

Much effort has been put in searching for signatures of Majorana fermions in solid state materials. One-dimensional semiconductor nano-wires with strong SO coupling under a magnetic field proximity to a s-wave superconductor have been proposed theoretically to host MF at both ends of the wire [4–6], and also studied experimentally [7–11]. Similar ideas have been proposed in 2D systems where chiral MFs exist at the edges of spin-triplet, p -wave (odd-parity) superconductors [12–14].

While realization of the above systems relies on TRS breaking by the Zeeman field, time-reversal invariant topological superconductors (TRITOPs) [15–18] has recently been proposed to host two time-reversal pairs of helical MFs at edges in repulsively interacting SO coupled nano-wire proximity to either a s-wave [6, 16] or a d -wave [19] superconductor at each end of the wire. Proposals to realize TRITOPs in 2D systems include the spin-triplet $p_x \pm ip_y$ superconductors [15], the bi-layer Rashba system [20], and in exciton condensates [21].

In this letter, we suggest a novel mechanism for realizing helical Majorana fermions in 2D topological superconductors with spin-singlet and TRS-breaking pairing gap—by directly doping correlated 2D quantum spin

Hall insulators (QSHIs or 2D TIs) [22, 23]. A paradigmatic model for QSHIs is the Kane-Mele (KM) model [23, 24], which shows a non-trivial Z_2 topological (or spin Chern) number and supports helical topological edge states protected by TRS. The half-filled KM model with strong electron correlations is in the Mott-insulating (MI) phase [25], while superconductivity appears upon doping. Attractive candidates to realize correlated KM model include: graphene with enhanced SO coupling ($\sim 20meV$) by doping with heavy adatoms, such as indium or thallium [26], Iridium-based honeycomb compounds X_2IrO_3 ($X = Na$ or Li) with strong SO coupling and electron correlations [25, 27].

Via renormalized mean-field theory (RMFT) approach [28], we find the spin-singlet TRS breaking $d_{x^2-y^2} + id_{xy}$ -wave superconductivity to appear at the ground state where the chiral edge states have been shown to occur [29]. Surprisingly, for sufficiently large SO coupling, instead of chiral edge states, we find zero-energy helical MFs to appear at each ribbon edge. We further show that the system exhibits a non-trivial Z_2 topological invariant, which supports helical MFs at edges despite the presence of TRS breaking superconductivity. This seemingly un-expected feature comes as a result of persistence of spin-Chern phase in the pure Kane-Mele model in the superconducting state at finite dopings. The competition between SO coupling and chiral d -wave superconductivity leads to a novel spin-Chern to chiral topological quantum phase transition.

Model Hamiltonian. The Hamiltonian of the Kane-

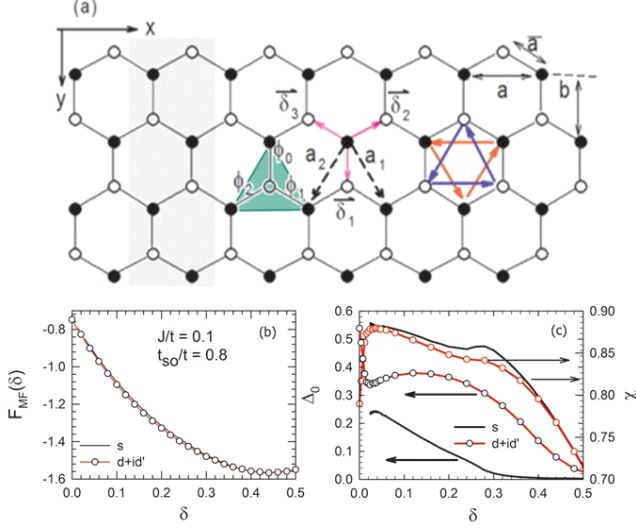


FIG. 1: (Color online) (a). Honeycomb lattice of a finite-sized zigzag ribbon of the tight-binding Kane-Mele t-J model with the ribbon size $N = 8$ being twice the number of zigzag chains along x -axis. Nearest-neighbor and next-nearest-neighbor lattice vectors are $\delta_{\alpha=1,2,3}$, $\mathbf{a}_{i=1,2}$ with an unit length of $\bar{\mathbf{a}}, \mathbf{a}$, respectively. We set $\mathbf{a} = 1$ here. The gray shaded region represents for the super-unit-cell of the zigzag ribbon, which repeats itself along x -axis. The filled (open) dots stand for the sites on sub-lattice $A(B)$. The three phases for $d + id'$ pairing gap are defined (see shaded green triangle) as: $\phi_0 = 0, \phi_{1(2)} = -(+)2\pi/3$. (b). Mean-field free energy F_{MF} versus doping δ of doped Kane-Mele model on 2D periodic lattice for extended s -wave and $d + id'$ -wave superconducting pairing symmetries. (c). Mean-field variables Δ_0 (strength of pairing gap) and χ -field versus doping for (b). The parameters used in (b) and (c) are: $J/t = 0.1$, $t_{SO}/t = 0.8$.

Mele t-J (KM-tJ) model is given by [23]:

$$\begin{aligned}
 H &= H_{KM} + H_J, \\
 H_{KM} &= -tg_t \sum_{\langle ij \rangle, \alpha} c_i^{\dagger \alpha} c_j^{\alpha} - \mu \sum_{i, \alpha} c_i^{\dagger \alpha} c_i^{\alpha}, \\
 &+ i \frac{t_{SO}}{3} \sum_{\langle\langle ij \rangle\rangle, \alpha} \nu_{ij} c_i^{\dagger \alpha} \sigma^z c_j^{\alpha} + h.c. \\
 H_J &= Jg_s \sum_{\langle i, j \rangle} (\vec{S}_i \cdot \vec{S}_j - \frac{1}{4} n_i n_j) \quad (1)
 \end{aligned}$$

where $\alpha = \uparrow, \downarrow$ stands for the spin index, $\langle i, j \rangle$ and $\langle\langle i, j \rangle\rangle$ refer to the nearest-neighbor (NN) and next-nearest-neighbor (NNN) sites, respectively (see Fig. 1 (a)). Here, $\nu_{ij} = 1$ for $i, j \in A$ and $\nu_{ij} = -1$ for $i, j \in B$ in the SO coupling; \vec{S}_i refers to the electron spin operator on site i , defined as: $\vec{S}_i = 1/2 \sum_{\alpha, \beta = \uparrow, \downarrow} c_i^{\dagger \alpha} \vec{\sigma}_{\alpha\beta} c_i^{\beta}$, $n_i = \sum_{\alpha} c_i^{\dagger \alpha} c_i^{\alpha}$ is the electron density operator, and the anti-ferromagnetic spin-exchange coupling $J \sim \frac{4t^2}{U}$ can

be derived via the second-order perturbation from the Kane-Mele Hubbard model in the limit of a strong on-site Coulomb repulsion $U \gg t$ [30].

The H_J term has been known to favor the spin-singlet pairing. To address superconductivity of the model, we apply RMFT based on Gutzwiller projected single-occupancy constraint due to the proximity of the Mott insulating ground states, known to well describe the ground state of d -wave cuprate superconductors [28]. As a result, the hopping t term acquires a reduction factor g_t at a finite doping δ : $t \rightarrow tg_t$ with $g_t = 2\delta/(1 + \delta)$, while the spin-exchange J term gets enhanced by a factor g_s : $J \rightarrow g_s J$ with $g_s = 4/(1 + \delta)^2$. The spin-exchange J term within RMFT reads: $H_J = H_{\chi} + H_{\Delta} + H_{const}$, $H_{\chi} = \sum_{i, \alpha, a} \chi_{\delta_a} c_i^{\dagger \alpha} c_{i+\delta_a}^{\alpha} + h.c.$, $H_{\Delta} = \sum_{i, a} \Delta_{\delta_a} [c_i^{\dagger \uparrow} c_{i+\delta_a}^{\dagger \downarrow} - c_i^{\dagger \downarrow} c_{i+\delta_a}^{\dagger \uparrow}] + h.c.$, $H_{const} = N_s \sum_a [\frac{|\chi_{\delta_a}|^2}{\frac{3}{4}g_s J} + \frac{|\Delta_{\delta_a}|^2}{\frac{3}{4}g_s J}] - 2N_s \mu \delta$ where $a = 1, 2, 3$, N_s is the total number of sites, $\chi_{\delta_a} = -\frac{3}{4}g_s \sum_{\alpha} J \langle c_i^{\dagger \alpha} c_{i+\delta_a}^{\alpha} \rangle$, $\Delta_{\delta_a} = -\frac{3}{4}g_s J \sum_{\alpha, \beta = \uparrow, \downarrow} \epsilon_{\alpha\beta} \langle c_i^{\alpha} c_{i+\delta_a}^{\beta} \rangle$, and $\epsilon_{\alpha\beta} = i\sigma_{\alpha\beta}^y$. Based on the C_{6v} symmetry of the underlying lattice, the pairing symmetry of $\Delta_{\delta_{a=1,2,3}}$ may take the following forms [31]: (i) extended s -wave: $\Delta_{\delta_a} = \Delta_{\delta_a}^s = \Delta_0$, (ii) $d_{x^2-y^2} + id_{xy}$ -wave (denoted also as $d + id'$): $\Delta_{\delta_a} = \Delta_{\delta_a}^{d+id'} = \Delta_0 e^{i\phi_{a-1}}$ with $\phi_0 = 0, \phi_{1(2)} = -(+)2\pi/3$ (see Fig. 1) [32]. The Fourier transformed pairing gap Δ_k for a periodic 2D lattice reads: $\Delta_k = \sum_{a=1,2,3} \Delta_{\delta_a} e^{i\vec{k} \cdot \delta_a}$.

The mean-field Hamiltonian $H_k = \psi_k^{\dagger} \mathcal{M}_k \psi_k$ on a periodic lattice in the basis of $\psi_k = (c_{A,k}^{\uparrow}, c_{B,k}^{\uparrow}, c_{A,k}^{\downarrow}, c_{B,k}^{\downarrow}, c_{A,-k}^{\uparrow}, c_{B,-k}^{\uparrow}, c_{A,-k}^{\downarrow}, c_{B,-k}^{\downarrow})^T$ is given by the 8×8 matrix \mathcal{M}_k :

$$\begin{aligned}
 \mathcal{M}_k &= \begin{pmatrix} \hat{h}_k & \hat{\Delta}_k \\ \hat{\Delta}_k^{\dagger} & -\hat{h}_{-k}^* \end{pmatrix}, \hat{h}_k = \begin{pmatrix} h_k^{\dagger} & \\ & \hat{h}_k \end{pmatrix}, \hat{\Delta}_k = \begin{pmatrix} 0 & \bar{\Delta}_k \\ -\bar{\Delta}_k & 0 \end{pmatrix}, \\
 h_k^{\pm} &= \begin{pmatrix} \pm\gamma_k - \mu & \epsilon_k \\ \epsilon_k^* & \mp\gamma_k - \mu \end{pmatrix}, \bar{\Delta}_k = \begin{pmatrix} 0 & \Delta_k \\ \Delta_{-k} & 0 \end{pmatrix} \\
 \gamma_k &= \frac{2}{3} t_{SO} [-\sin(k_y) + 2 \cos(\sqrt{3}k_x/2) \sin(k_y/2)], \\
 \epsilon_k &= -(tg_t + \chi) \sum_{a=1,2,3} e^{i\vec{k} \cdot \delta_a}. \quad (2)
 \end{aligned}$$

The Hamiltonian Eq. (2) possesses both the Particle-hole (PH) symmetry: $\mathcal{C}^{-1} \mathcal{M}_k \mathcal{C} = -\mathcal{M}_{-k}$, $\mathcal{C} = \tau^x K$ (with τ^x being the Pauli matrix on particle-hole space where K stands for complex conjugation as well as sublattice symmetry: $\mathcal{M}_k \rightarrow \mathcal{M}_{-k}$ for $c_{A,k} \rightarrow c_{B,k}$ [31]). The matrix \hat{h}_k , describing the KM model, shows TRS: $\mathcal{T}^{-1} \hat{h}_k \mathcal{T} = \hat{h}_{-k}$ where $\mathcal{T} = i\sigma^y K$ is the time-reversal operator taking $(c_k^{\uparrow}, c_k^{\downarrow})$ to $(c_{-k}^{\downarrow}, -c_{-k}^{\uparrow})$. However, \mathcal{M}_k breaks the TRS for $d + id'$ superconducting order parameter: $\Delta_k^{d+id'} = \cos(\pi/3) \Delta_{d_{x^2-y^2}}(k) + i \sin(\pi/3) \Delta_{d_{xy}}(k)$ with $\Delta_{d_{x^2-y^2}}(k) = 2\Delta_0 (e^{-ik_y/\sqrt{3}} - e^{ik_y/2} \cos(k_x/2\sqrt{3}))$, $\Delta_{d_{xy}}(k) = -2i\Delta_0 e^{ik_y/2} \sin(k_x/2\sqrt{3})$, and

$\mathcal{T}^{-1}\mathcal{M}_k^{d+id'}\mathcal{T} \neq \mathcal{M}_{-k}^{d+id'}$. The mean-field free energy reads: $F_{MF} = -\frac{2T}{N_s} \sum_k \ln[\cosh(\frac{E_k}{2T})] + \frac{H_{const}}{N_s}$ with $E_k > 0$ being positive eigenvalues and N_s the number of sites. We diagonalized the mean-field Hamiltonian H_k on a finite-sized zigzag ribbon with $N_s = N/2$ zigzag chains and $N = 56$ is set as the total number of sites along y -axis throughout the paper.

Results. The mean-field variables are solved self-consistently by minimizing the free energy both for a periodic lattice and a finite-sized ribbon. On a 2D periodic lattice, the results as a function of doping are shown in Fig. 1(b) and (c). Compared to the TRS extended s -wave, we find $d_{x^2-y^2} + id_{xy}$ -wave pairing is the ground state [32]. Same pairing symmetry has been reported in superconducting phase of the doped graphene in the absence of the spin-orbit coupling [29, 31, 33, 34], which was argued to support two co-propagating chiral edge states at low energies with a non-trivial topological winding number $N_{TKNN} = \pm 2$ [35]. The superconducting transition temperature T_c is estimated as $T_c \sim g_t \Delta_0$.

On a finite-sized zigzag ribbon and at a generic doping, the Bogoliubov quasi-particle dispersion shows four doubly-degenerate bulk bands (due to the S_z symmetry of our Hamiltonian) grouped in two pairs (see Fig. 2(a)); it satisfies the particle-hole symmetry with 2π periodicity: $E(k_x - \pi) = -E(k_x + \pi)$. At low dopings, the normal state Fermi surfaces enclose the Dirac points $K_{\pm} = (\frac{2\pi}{\sqrt{3}}, \pm \frac{2\pi}{3})$ (see Fig. 2 (b)); the $d + id'$ pairing strength is weak near K_- [32]. Surprisingly, in the regime of a strong SO coupling and weak pairing ($\Delta^{d+id'} \ll \sqrt{3}t_{SO}$), we find the low energy excitations of our model support helical MFs at edges instead of chiral edge states as expected for a chiral d -wave superconductor. On a finite-sized zigzag ribbon, we find two Dirac-dispersed lines intersecting at momenta $k_x^{MF} \sim 2\pi/3, 4\pi/3$ where the Bogoliubov quasi-particle excitation energy vanishes, $E(k_x^{MF}) = 0$ (see Fig. 2(a) and Fig. 3(a))[36]. Near each of these gapless points, two pairs of two-fold degenerate states are generated via intersecting the two Dirac lines by a constant energy at two momentum points $k_{x1(x2)}^{MF}$, denoted as: $\Psi_{1(2),j=1,2}^{MF}$. These four degenerate states are located at the same edge. However, $\Psi_{1,j}^{MF}$ and $\Psi_{2,j}^{MF}$ are counter-propagating, while $\Psi_{j,1}^{MF}$ and $\Psi_{j,2}^{MF}$ are co-propagating (see Fig. 3(b)). In the basis of $\bar{\Psi} = [\Pi_i c_i^{\uparrow}, \Pi_i c_i^{\downarrow}, \Pi_i c_i^{\uparrow\uparrow}, \Pi_i c_i^{\downarrow\downarrow}]$ with $i = 1 \dots N$, the square magnitudes of two pairs of degenerate eigenstate wave-functions associated with the same k_x^{MF} , defined as $|\Psi(i)|^2 \equiv |\Psi_{j=1,2}^{R/L}(i)|^2 \equiv (|u(i)|^2, |\tilde{u}(i)|^2, |\tilde{v}(i)|^2, |v(i)|^2)_j^{R/L}$, exhibit an exponential decay from both edges into the bulk, where R/L refers to the right/left moving state, and $u(i), \tilde{u}(i), \tilde{v}(i), v(i)$ are the corresponding matrix elements.

These features are clearly different from the co-propagating chiral edge states realized either in the chiral d -wave superconductivity in doped graphene or

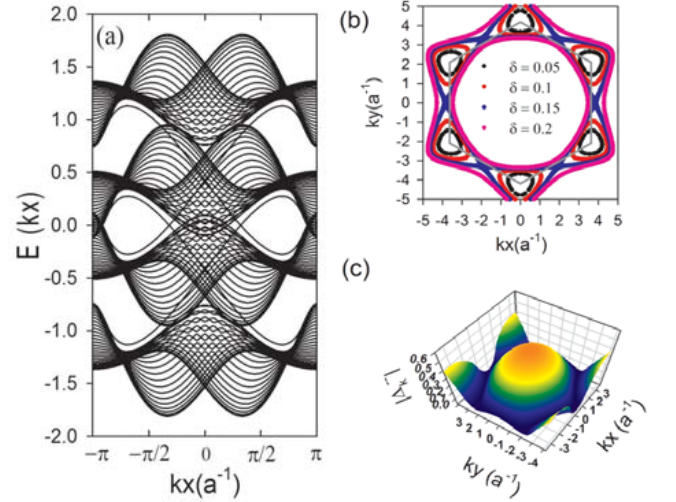


FIG. 2: (Color online) (a) The Bogoliubov dispersion $E(k_x)$ (in unit of t) of doped KM-tJ model on a zigzag ribbon with $N = 56$ for $J/t = 0.1$, $t_{SO}/t = 0.8$, and $\delta = 0.05$. (b). The spin-up Fermi surfaces in the normal state of the Kane-Mele model on 2D periodic lattice for $t_{SO}/t = 1$ at various dopings. The spin-down Fermi surfaces are obtained via $K_+ \rightarrow K_-$. (c) The 3D density plot for the effective intra-band superconducting gap function $|\Delta_k^-|$ of the Kane-Mele model on 2D periodic lattice (see text and Ref. 37).

by proximity of a s -wave superconductor to a quantum anomalous Hall insulators [38]. Instead, the edge states we find fit well to the helical MFs described by the linearly-dispersed Hamiltonian defined by the Bogoliubov quasi-particle operators $\gamma_k^{R(L)\tau}$ as: $H_{edge} = \sum_{\bar{k}, \tau=\uparrow, \downarrow} |\bar{k}| (\gamma_{\bar{k}}^{\uparrow R\tau} \gamma_{\bar{k}}^{R\tau} - \gamma_{\bar{k}}^{\downarrow L\tau} \gamma_{\bar{k}}^{L\tau})$, $\gamma_{\bar{k}}^{R\tau} = u_{\bar{k}, \bar{i}}^{\tau} c_{\bar{k}, \bar{i}}^{\uparrow} + \tilde{u}_{\bar{k}, \bar{i}}^{\tau} c_{\bar{k}, \bar{i}}^{\downarrow} + \tilde{v}_{\bar{k}, \bar{i}}^{\tau} c_{-\bar{k}, \bar{i}}^{\uparrow} + v_{\bar{k}, \bar{i}}^{\tau} c_{-\bar{k}, \bar{i}}^{\downarrow}$, $\gamma_{\bar{k}}^{L\tau} = -v_{\bar{k}, \bar{i}}^{\tau} c_{-\bar{k}, \bar{i}}^{\uparrow} + \tilde{v}_{\bar{k}, \bar{i}}^{\tau} c_{-\bar{k}, \bar{i}}^{\downarrow} - \tilde{u}_{\bar{k}, \bar{i}}^{\tau} c_{\bar{k}, \bar{i}}^{\uparrow} + u_{\bar{k}, \bar{i}}^{\tau} c_{\bar{k}, \bar{i}}^{\downarrow}$, where $\bar{k} = k - k_x^{MF}$, $k \equiv k_x$, $\gamma_{\bar{k}}^{\alpha\tau}$ with $\alpha = L, R$ refers to the Bogoliubov quasi-particle destruction operator defined by the coherence factors $u_{\bar{k}, \bar{i}}^{\tau}, \tilde{u}_{\bar{k}, \bar{i}}^{\tau}, \tilde{v}_{\bar{k}, \bar{i}}^{\tau}, v_{\bar{k}, \bar{i}}^{\tau}$, corresponding to the right-moving quasi-particle with “pseudo-spin” $\tau = \uparrow (\downarrow)$, and the summation over repeated site index $\bar{i} = 1, \dots, N$ is implied; similarly for $\gamma_{\bar{k}}^{L\tau}$. The pair of the degenerate wavefunctions $\Psi_{j=1(2)}^{R(L)}(\bar{i})$ at $k_{x1}^{MF}(k_{x2}^{MF})$ can be expressed as $\Psi^{R(L), \uparrow(\downarrow)}(\bar{i})$, formed by the coherence factors: $\Psi^{R, \uparrow}(\bar{i}) = (u_{\bar{k}, \bar{i}}^{\uparrow}, \tilde{u}_{\bar{k}, \bar{i}}^{\uparrow}, \tilde{v}_{\bar{k}, \bar{i}}^{\uparrow}, v_{\bar{k}, \bar{i}}^{\uparrow})$, $\Psi^{L, \downarrow}(\bar{i}) = (-v_{\bar{k}, \bar{i}}^{\downarrow}, \tilde{v}_{\bar{k}, \bar{i}}^{\downarrow}, -\tilde{u}_{\bar{k}, \bar{i}}^{\downarrow}, u_{\bar{k}, \bar{i}}^{\downarrow})$; similarly for the other doublet $\Psi^{R(L), \downarrow(\uparrow)}(\bar{i})$. It is clear from Fig. 3 (b) that the edge states ($\Psi^{R(L), \uparrow(\downarrow)}, \Psi^{L(R), \downarrow(\uparrow)}$) (as well as the Bogoliubov operators ($\gamma_{\bar{k}}^{R\uparrow(L\downarrow)}, \gamma_{\bar{k}}^{L\downarrow(R\uparrow)}$)) form pairs (see pink (blue) curve in Fig. 3(b) for $|\Psi^{R, \uparrow}(\bar{i})|^2 (|\Psi^{L, \downarrow}(\bar{i})|^2)$). Furthermore, these Bogoliubov operators with linear dispersion satisfy $\gamma_{-\bar{k}}^{\uparrow}(-E) = \gamma_{\bar{k}}^{\downarrow}(E)$ with $\tilde{k} \equiv k - \pi$ via PH symmetry (see top and bottom panels of Fig. 3(b)). Hence, they can be regarded as examples of helical MFs at edges

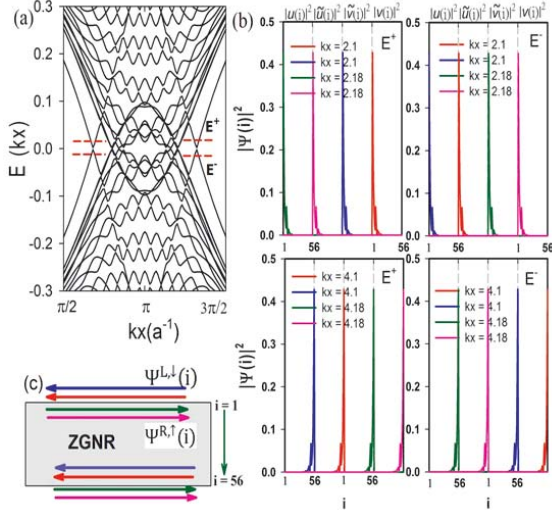


FIG. 3: (Color online) (a) Bogoliubov excitation spectrum of Fig. 2(a) near zero energy. (b) The square magnitudes of two pairs of degenerate eigen-vectors $|\Psi^{R/L,\tau}(i)|^2 \equiv (|\tilde{u}(i)|^2, |\tilde{v}(i)|^2, |\tilde{w}(i)|^2, |v(i)|^2)$ (see text) for a fixed eigenenergy $E = E^\pm = \pm 0.014t$ with i running (left to right) from $i = 1$ (top edge) to $i = 56$ (bottom edge), corresponding to the helical Majorana fermions. Physical parameters are the same as in (a). (c) Schematic plot of the helical edge states in (b) for $E = E^+$ where same color in (b) and (c) refers to the same state. Here, ZGNR refers to the Kane-Mele zigzag nano-ribbon.

[15]; the MF zero-modes occur at $k = k_x^{MF}$ (or $\bar{k} = 0$) where $\gamma_{\bar{k}=0}^{\alpha\tau} = \gamma_{\bar{k}=0}^{\dagger\alpha\tau}$. These helical MFs are protected by an additional P-H symmetry: $\gamma_{-\bar{k}}(E) = \gamma_{\bar{k}}^\dagger(E)$ (see Fig. 3(b)). Our seemingly unexpected results have roots in the competition between TRS SO coupling and TRS breaking chiral d -wave superconductivity. We find the TRS protected Z_2 QSH insulating phase of the pure undoped Kane-Mele model persists up to a finite doping and a finite pairing gap in the chiral d -wave superconducting phase.

To gain more understanding, we compute the Z_2 topological invariant (spin Chern number) $N_W = \frac{1}{2}(C_n - C_{\bar{n}})$ with $C_n = \frac{1}{2\pi i} \int_{k \in BZ} F_{12}(k)$ where the integral is done in the first Brillouin zone (BZ), the field strength $F_{12}(k)$ and the associated Berry's connection $A(k)$ are defined as: $F_{12}(k) \equiv \partial_1 A_2(k) - \partial_2 A_1(k)$ and $A_\mu = \langle n(k) | \partial_\mu | n(k) \rangle$ with $|n(k)\rangle$ being the normalized eigenvector of the n th band [39]. $C_{\bar{n}}$ is defined similarly with \bar{n} being the corresponding degenerate band associated with the n -th band via the transformation $S_z = \uparrow \rightarrow \downarrow$. In the strong SO coupling regime, $t_{SO} \gg \Delta_0$ and for a sizable range of doping around 1/2-filling, the spin-Chern phase prevails and we find $C_n = -C_{\bar{n}}$ or $N_W = \pm 1$ [37], same result as that for the Z_2 TRITOPs supporting helical MFs at edges [1, 15, 40, 41]. In this limit, our system is well approximated by the effective spin-singlet $p_x \pm ip_y$

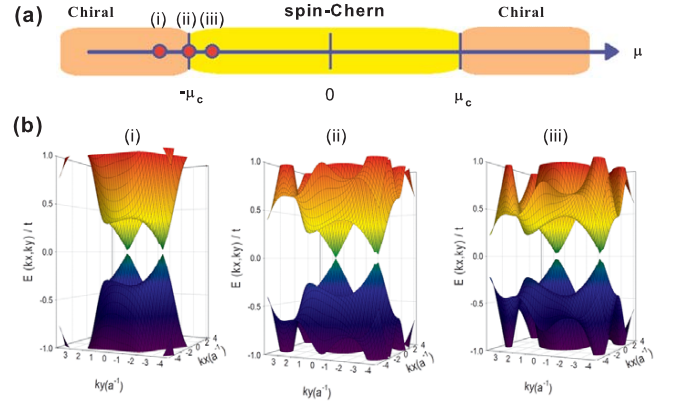


FIG. 4: (Color online) (a) Topological phase diagram of doped Kane-Mele t -J model on 2D periodic honeycomb lattice as a function of μ for fixed $\Delta_0/t = 0.3$, $t_{SO}/t = 0.9$. Here, we set $\chi = 0$, $g_t = g_s = 1$ for simplicity, and $\pm\mu_c \sim \pm\sqrt{3}t_{SO}$ refers to the critical chemical potential at the spin-Chern-chiral phase transition. The values of Δ_0 and μ are tuned in a non-self-consistent way. (b) Energy dispersion of the two bulk bands close to zero energy. The bulk band gap closes at the phase boundary $\mu \sim -\mu_c$ at one Dirac point (case (ii) with $\mu/t = -1.409$, $\delta = 0.43$), while it remains finite on either of the two phases (cases (i) with $\mu/t = -1.8$, $\delta = 0.58$ and case (iii) with $\mu/t = -1.2$, $\delta = 0.34$).

superconductivity near the two Dirac points K_\pm . This can be seen when re-expressing the superconducting pairings in terms of the electron operators $\psi_{\pm,k}$ which diagonalize the tight-binding KM Hamiltonian [32, 37]. In this basis, the intra-band pairing $\Delta_k^- \psi_{-,k}^\dagger \psi_{-,k}^\dagger$ dominates at ground state (see Fig. 2 (c) and Ref. 37). Near K_\pm points with $q_\pm = K_\pm + (\pm q_x + q_y)$, we find $\Delta_{q_\pm}^- \sim \pm\Delta_0(q_y \pm iq_x)$, resembling the case of a TRITOPs. In the opposite limit for $t_{SO} \ll \Delta_0$ or sufficiently large doping where the chiral d -wave pairing dominates, however, we recover the chiral superconductivity: $N_W = 0$ and $C_n = C_{\bar{n}} = 1$, equivalent to the case of doped graphene [29, 31]. A novel spin-Chern-to-chiral topological quantum phase transition is found as Δ_0/t_{SO} or μ/t_{SO} is varied [42]. The generic phase diagram by tuning μ (in a non-self-consistent way) at a fixed Δ_0/t_{SO} is shown in Fig.4 (a). For $\Delta_0 \ll t_{SO}$, we find the critical values of μ being at $\mu = \pm\mu_c \sim \pm\sqrt{3}t_{SO}$. The bulk band gap closes only at the phase transition, while it remains open in either phase [42–44] (see Fig. 4(b)). The similar persistence of spin-Chern phase in a TRS breaking magnetic field has been observed experimentally in Ref. 45. The spin-Chern phase of our system belongs to class D topological superconductors, distinct from the TRITOPs [19, 46, 47].

Conclusions. We demonstrate here for the first time a 2D *spin-singlet* topological superconductor with non-trivial spin Chern number in doped correlated Kane-Mele model, which supports helical counter-propagating Majorana zero modes despite the $d+id'$ superconducting

pairing gap breaks TRS. This seemingly unexpected feature comes as a result of persistence of spin-Chern phase of the pure Kane-Mele model in the superconducting state upon doping. As $T \rightarrow 0$, distinct differential conductance spectrum for each pair of Majorana zero mode through differential Andreev conductance in the normal-metal/superconducting (NS) junction is expected[29, 31].

We thank Y. Oreg, A. Haim, S.M. Huang, P.A. Lee, C.Y. Mou, K.T. Law, M. Sato, I.C. Fulga for helpful discussions. This work is supported by the NSC grant No.98-2918-I-009-06, No.98-2112-M-009-010-MY3, the NCTU-CTS, the MOE-ATU program, the NCTS of Taiwan, R.O.C. (CHC), and NSFC grant No. 11274269 (FCZ).

-
- [1] M. Z. Hasan, C. L. Kane, Rev. Mod. Phys., **82**, 3045 (2010).
- [2] X.L. Qi, S.C. Zhang, Rev. Mod. Phys. **83**, 1057 (2011).
- [3] Jason Alicea, Rep. Prog. Phys. **75**, 076501 (2012).
- [4] R. Lutchyn, J. Sau, and S. Das Sarma, Phys. Rev. Lett. **105**, 77001 (2010).
- [5] Y. Oreg, G. Refael, and F. Von Oppen, Phys. Rev. Lett. **105**, 177002 (2010).
- [6] E. Gaidamauskas, J. Paaske, and K. Flensberg, Phys. Rev. Lett. **112**, 126402 (2014).
- [7] V. Mouril, K. Zuo, S. Frolov, S. Plissard, E. Bakkers, and L. Kouwenhoven, Science **336**, 1003 (2012).
- [8] A. Das, Y. Ronen, Y. Most, Y. Oreg, M. Heiblum, and H. Shtrikman, Nat. Phys. **8**, 887 (2012).
- [9] H. O. H. Churchill, V. Fatemi, K. Grove-Rasmussen, M. T. Deng, P. Caroff, H. Q. Xu, C. M. Marcus, Phys. Rev. B **87**, 241401(R) (2013).
- [10] M.T. Deng, C.L. Yu, G.Y. Huang, M. Larsson, P. Caro, and H.Q. Xu, Nano Lett. **12**, 6414 (2012).
- [11] A.D.K. Finck, D.J. Van Harlingen, P.K. Mohseni, K. Jung, and X. Li, Phys. Rev. Lett. **110**, 126406 (2013).
- [12] M. Sato, S. Fujimoto, Phys. Rev. B **79** (2009).
- [13] J.D. Sau, R.M. Lutchyn, S. Tewari, and S. Das Sarma, Phys. Rev. Lett. **104**, 040502 (2010).
- [14] L. Fu, and C.L. Kane, Phys. Rev. Lett. **100**, 096407 (2008).
- [15] X.-L. Qi, T. L. Hughes, S. R., and S.-C. Zhang, Phys. Rev. Lett. **102**, 187001 (2009).
- [16] A. Haim, A. Keselman, E. Berg and Y. Oreg, Phys. Rev. B **89**, 220504(R) (2014).
- [17] E. Dumitrescu, and S. Tewari, Phys. Rev. B **88**, 220505(R) (2013).
- [18] F. Zhang, C.L. Kane, and E.J. Mele, Phys. Rev. Lett. **111**, 056402 (2013).
- [19] C. L.M. Wong and K.T. Law, Phys. Rev. B **86**, 184516 (2012).
- [20] S. Nakosai, Y. Tanaka, N. Nagaosa, Phys. Rev. Lett. **108**, 147003 (2012).
- [21] B. Seradjeh, Phys. Rev. B **86**, 121101(R) (2012).
- [22] F.D.M. Haldane, Phys. Rev. Lett. **61**, 2015 (1988).
- [23] C.L. Kane and E.J. Mele, Phys. Rev. Lett. **95**, 146802 (2005).
- [24] C.L. Kane and E.J. Mele, Phys. Rev. Lett. **95**, 226801 (2005).
- [25] S. Rachel and K. Le Hur, Phys. Rev. B **82**, 075106 (2010).
- [26] C. Weeks, J. Hu, J. Alicea, M. Franz, R. Wu, Phys. Rev. X **1**, 021001 (2011).
- [27] A. Shitade, H. Katsura, J. Kunes, X.-L. Qi, S.-C. Zhang, and N. Nagaosa, Phys. Rev. Lett. **102**, 256403 (2009); M. Jenderka, J. Barzola-Quiquia, Z. Zhang, H. Frenzel, M. Grundmann, and M. Lorenz, Phys. Rev. B **88**, 045111 (2013); M. Laubach, J. Reuther, R. Thomale, S. Rachel, arXiv:1312.2934 (un-published).
- [28] F.C. Zhang, C. Gros, T.M. Rice and H. Shiba, Supercond. Sci. Technol. **1** 36 (1988); F. C. Zhang and T. M. Rice, Phys. Rev. B **37**, 3759 (1988).
- [29] A. M. Black-Schaffer, Phys. Rev. Lett. **109**, 197001 (2012).
- [30] We neglect here a small ferromagnetic spin-exchange between NNN sites on the same sublattice arising from SO coupling t_{SO} , which may lead to spin-triplet pairing.
- [31] Y. Jiang, D.-X. Yao, E. W. Carlson, H.-D. Chen, and J.P. Hu, Phys. Rev. B **77**, 235420 (2008).
- [32] W. Wu, M.M. Scherer, C. Honerkamp, K. Le Hur, Phys. Rev. B **87**, 094521 (2013).
- [33] S. Pathak, V. B. Shenoy, and G. Baskaran, Phys. Rev. B **81**, 085431 (2010).
- [34] W.-S. Wang, Y.-Y. Xiang, Q.-H. Wang, F. Wang, F. Yang, D.-H. Lee, Phys. Rev. B **85**, 035414 (2012).
- [35] A. M. Black-Schaffer and C. Honerkamp, J. Phys.: Condens. Matter **26** (2014) 423201.
- [36] Due to large t_{SO}/Δ_0 ratio from our mean-field solution, we find bulk gap closes near $k_x = 0, \pi$ (see Fig. 2). This comes as spin-orbital gap of the pure Kane-Mele ribbon gets smaller near Γ point. Upon doping, the P-H symmetry of the bands is imposed, leading to the overlap between particle and hole bands near $k_x = 0, \pi$ for large t_{SO}/Δ_0 . We have checked numerically that all the states near $k_x = 0, \pi$ are indeed bulk states.
- [37] See Supplementary Materials for details.
- [38] X.-L. Qi, T. L. Hughes, S.-C. Zhang, Phys. Rev. B **82**, 184516 (2010).
- [39] T. F. Ukui, Y. H. Atsugai and H. S. Uzuki, J. Phys. Soc. Jpn., **74**, 1674 (2005).
- [40] The existence of two pairs of helical edge states via mean-field analysis agrees perfectly with the total spin Chern number being ± 2 via summing over N_W for all four filled bands.
- [41] A. P. Schnyder, S. Ryu, A. Furusaki, A. W. W. Ludwig, AIP Conf. Proc. 1134, 10 (2009).
- [42] The global topological phase diagram will be addressed elsewhere, see Shin-Ming Huang, Chung-Yu Mou and Chung-Hou Chung, (in preparation).
- [43] M. Ezawa, Y. Tanaka, N. Nagaosa, Scientific Reports, **3**, 2790 (2013).
- [44] Lunhui Hu *et al*, private communications.
- [45] L. Du, I. Knez, G. Sullivan, R.-R. Du, arXiv:1306.1925.
- [46] M. Sato, Phys. Rev. B **90**, 165114 (2014).
- [47] Due to the emergent spin-singlet $p_x \pm ip_y$ superconductor for large spin orbit coupling we expect that the effect of disorder induced backscattering is reduced, even though it is not strictly forbidden, due to the TRS breaking $d + id'$ superconductivity in the background. As a result the localization length (along the edge) of the counter propagating MF helical modes will be very long for moderate disorder scattering. However, these helical MFs are unstable against S_z -preserving scatterings.

Supplementary Materials for Helical Majorana fermions in $d_{x^2-y^2} + id_{xy}$ -wave topological superconductivity of doped correlated quantum spin Hall insulators

Shih-Jye Sun¹, Chung-Hou Chung^{2,3}, Yung-Yeh Chang², Wei-Feng Tsai⁴, and Fu-Chun Zhang^{5,6}

¹*Department of Applied Physics, National University of Kaohsiung, Kaohsiung, Taiwan, R.O.C.*

²*Electrophysics Department, National Chiao-Tung University, HsinChu, Taiwan, 300, R.O.C.*

³*Physics Division, National Center for Theoretical Sciences, HsinChu, Taiwan, 300 R.O.C.*

⁴*Department of Physics, National Sun Yat-Sen University, Kaohsiung, Taiwan, R.O.C.*

⁵*Department of Physics, Zhejiang University, Hangzhou, China*

⁶*Collaborative Innovation Center of Advanced Microstructures, Nanjing, China*

(Dated: August 31, 2021)

In the Supplementary Materials, we provide some of the details in the main text.

PACS numbers: 72.15.Qm, 7.23.-b, 03.65.Yz

I. THE HAMILTONIAN OF THE KANE-MELE T-J MODEL ON A ZIGZAG RIBBON

Here, we provide in details the Hamiltonian of the Kane-Mele t-J model on zigzag ribbon. The Hamiltonian matrix is $4N \times 4N$ in size with $N/2$ being the number of zigzag chains along x -axis. Each zigzag chain passes through either A sites or B sites. The ket state of the Hamiltonian is

$$|\Psi\rangle = (c_{1\uparrow}^+ c_{2\uparrow}^+ \cdots c_{N\uparrow}^+ c_{1\downarrow}^+ c_{2\downarrow}^+ \cdots c_{N\downarrow}^+ c_{1\uparrow} c_{2\uparrow} \cdots c_{N\uparrow} c_{1\downarrow} c_{2\downarrow} \cdots c_{N\downarrow})^T \quad (\text{I.1})$$

The Hamiltonian comprises three terms

$$H = H_0 + H_{so} + H_{\Delta}. \quad (\text{I.2})$$

Here, H_0 represents the nearest-neighbor hopping terms in the matrix form of $(\cdots c_{i\sigma}^+ \cdots)H(\cdots c_{j\sigma} \cdots)^T$, given by:

for $i = 1, 3, 5 \cdots N - 1$,

$$\begin{aligned} H_{0,\sigma\sigma}(i, i+1) &= -2t\cos\left(\frac{k}{2}\right), \\ H_{0,\sigma\sigma}(i+1, i) &= H_{0,\sigma\sigma}(i, i+1) \end{aligned} \quad (\text{I.3})$$

for $i = 2, 4, 6 \cdots N$,

$$\begin{aligned} H_{0,\sigma\sigma}(i, i+1) &= -t, \\ H_{0,\sigma\sigma}(i+1, i) &= H_{0,\sigma\sigma}(i, i+1), \end{aligned}$$

where $\sigma = \uparrow, \downarrow$ (+ or -), and $k = k_x$. The matrix elements of the form $(\cdots c_{i\sigma} \cdots)H(\cdots c_{j\sigma}^+ \cdots)^T$ is related to $(\cdots c_{i\sigma}^+ \cdots)H(\cdots c_{j\sigma} \cdots)^T$ by a minus sign. The H_{so} describes the intrinsic spin-orbit coupling with the follow-

ing matrix form:

for $i = 3, 5, 7 \cdots N - 3$

$$\begin{aligned} H_{so,\sigma\sigma}(i, i-2) &= \sigma \frac{2}{3} t_{so} \sin\left(\frac{k}{2}\right), \\ H_{so,\sigma\sigma}(i-2, i) &= H_{so,\sigma\sigma}(i, i-2), \\ H_{so,\sigma\sigma}(i, i+2) &= \sigma \frac{2}{3} t_{so} \sin\left(\frac{k}{2}\right), \\ H_{so,\sigma\sigma}(i+2, i) &= H_{so,\sigma\sigma}(i, i-2), \\ H_{so,\sigma\sigma}(i, i) &= -\sigma \frac{2}{3} t_{so} \sin(k); \end{aligned}$$

for $i = 4, 6, 8 \cdots N - 2$

$$\begin{aligned} H_{so,\sigma\sigma}(i, i-2) &= -\sigma \frac{2}{3} t_{so} \sin\left(\frac{k}{2}\right), \\ H_{so,\sigma\sigma}(i-2, i) &= H_{so,\sigma\sigma}(i, i-2), \\ H_{so,\sigma\sigma}(i, i+2) &= -\sigma \frac{2}{3} t_{so} \sin\left(\frac{k}{2}\right), \\ H_{so,\sigma\sigma}(i+2, i) &= H_{so,\sigma\sigma}(i, i-2), \\ H_{so,\sigma\sigma}(i, i) &= \sigma \frac{2}{3} t_{so} \sin(k); \end{aligned}$$

and the other matrix elements read

$$\begin{aligned} H_{so,\sigma\sigma}(1, 1) &= -\sigma \frac{2}{3} t_{so} \sin(k), \\ H_{so,\sigma\sigma}(2, 2) &= \sigma \frac{2}{3} t_{so} \sin(k), \\ H_{so,\sigma\sigma}(N-1, N-1) &= -\sigma \frac{2}{3} t_{so} \sin(k), \\ H_{so,\sigma\sigma}(N, N) &= \sigma \frac{2}{3} t_{so} \sin(k), \end{aligned} \quad (\text{I.4})$$

where the matrix elements with the abnormal order is minus the normal order elements. The H_{Δ} is the superconducting pairing gap with the matrix elements of the form $(\cdots c_{i,\sigma} \cdots)H(\cdots c_{j,-\sigma} \cdots)^T$ or $(\cdots c_{i,\sigma}^+ \cdots)H(\cdots c_{j,-\sigma}^+ \cdots)^T$,

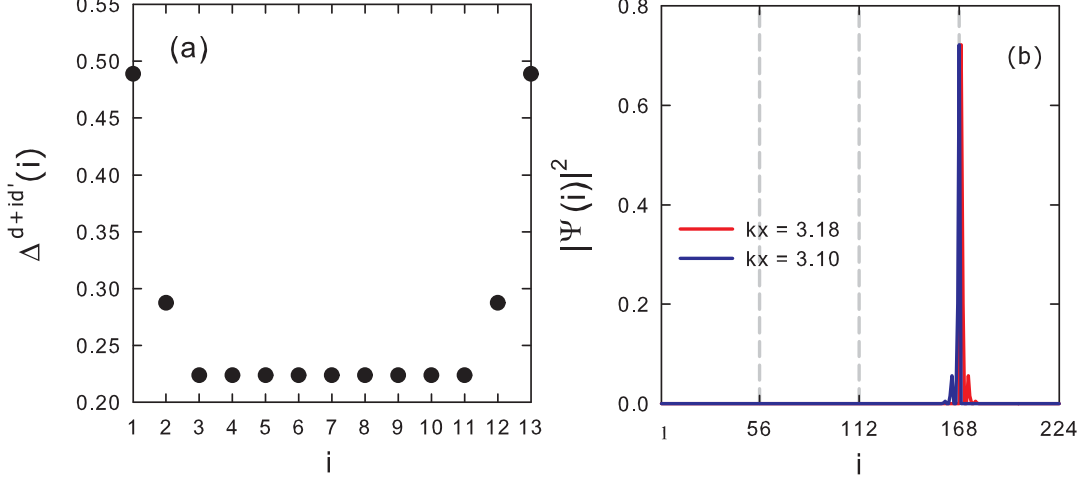


FIG. 1: (Color online) (a) Superconducting gap $\Delta^{d+id'}$ as a function of position in the zigzag ribbon for $N = 26$ (or $N/2 = 13$ zigzag chains). (b) Square magnitude of wave functions $|\Psi(i)|^2$ at the edge in the superconducting states with an energy $E/t = -0.613$ as a function of position $i = 1 \cdots N$ in the zigzag ribbon with $N = 56$. Here, we take the uniform mean-field solution for $\Delta^{d+id'}(i) = 0.22$ for $N = 56$. The parameters used in (a) and (b) are: $J/t = 0.1$, $\delta = 0.15$, $t_{SO}/t = 0.5$.

given by:

for $i = 1, 3, 5 \cdots N - 1$

$$H_{\Delta}(i, i - 1 + 3N) = \Delta_0$$

$$H_{\Delta}(i - 1, i + 3N) = \Delta_0$$

$$H_{\Delta}(i, i + 1 + 3N) = \Delta_1 + \Delta_2$$

$$H_{\Delta}(i + 1, i + 3N) = \Delta_1 + \Delta_2$$

similarly

$$H_{\Delta}(i + N, i - 1 + 2N) = -\Delta_0$$

$$H_{\Delta}(i - 1 + N, i + 2N) = -\Delta_0$$

$$H_{\Delta}(i + N, i + 1 + 2N) = -\Delta_1 - \Delta_2$$

$$H_{\Delta}(i + 1 + N, i + 2N) = -\Delta_1 - \Delta_2$$

$$H_{\Delta}(i + 2N, i - 1 + N) = H_{\Delta}(i + N, i - 1 + 2N)^*$$

$$H_{\Delta}(i - 1 + 2N, i + N) = H_{\Delta}(i - 1 + N, i + 2N)^*$$

$$H_{\Delta}(i + 2N, i + 1 + N) = H_{\Delta}(i + N, i + 1 + 2N)^*$$

$$H_{\Delta}(i + 1 + 2N, i + N) = H_{\Delta}(i + 1 + N, i + 2N)^*$$

$$H_{\Delta}(i + 3N, i - 1) = H_{\Delta}(i, i - 1 + 3N)^*$$

$$H_{\Delta}(i - 1 + 3N, i) = H_{\Delta}(i - 1, i + 3N)^*$$

$$H_{\Delta}(i + 3N, i + 1) = H_{\Delta}(i, i + 1 + 3N)^*$$

$$H_{\Delta}(i + 1 + 3N, i) = H_{\Delta}(i + 1, i + 3N)^*,$$

and the other matrix elements read

$$H_{\Delta}(1, 2 + 3N) = \Delta_1 + \Delta_2$$

$$H_{\Delta}(2, 1 + 3N) = H_{\Delta}(1, 2 + 3N)$$

$$H_{\Delta}(1 + N, 2 + 2N) = -H_{\Delta}(1, 2 + 3N)$$

$$H_{\Delta}(2 + N, 1 + 2N) = -H_{\Delta}(2, 1 + 3N)$$

$$H_{\Delta}(1 + 2N, 2 + N) = H_{\Delta}(1 + N, 2 + 2N)^*$$

$$H_{\Delta}(2 + 2N, 1 + N) = H_{\Delta}(2 + N, 1 + 2N)^*$$

$$H_{\Delta}(1 + 3N, 2) = H_{\Delta}(1, 2 + 3N)^*$$

$$H_{\Delta}(2 + 3N, 1) = H_{\Delta}(2, 1 + 3N)^*$$

(I.5)

where Δ_0 is the pairing order $\langle c_{i,\sigma} c_{j,-\sigma} \rangle$, Δ_0 , Δ_1 and Δ_2 correspond to the pairing order parameters carrying different phases $0, \frac{2\pi}{3}$ and $\frac{4\pi}{3}$ in $d+id'$ -wave superconducting states, respectively.

II. ADDITIONAL RESULTS OF THE KANE-MELE T-J MODEL ON A ZIGZAG RIBBON

Here, we provide additional results based on our numerical calculations on the doped Kane-Mele $t-J$ model via RMFT.

A. Superconducting states at the edges

In the Bogoliubov quasi-particle spectrum on the zigzag ribbon (see Fig. 2 in the main text), we find two linear-dispersed spectrum crossed at $k_x \sim \pi$ with the energy $E = \pm E_0$ ($E_0 > 0$). They are closely related to the edge states of the pure Kane-Mele model. The negative energy state ($E < 0$) corresponds to the superconducting state at the edges as it supports finite values in superconducting order parameter Δ_0 at the edges and their corresponding eigen-vectors are distributed mainly at the edges (see Fig. 1 (b)).

To investigate further the position dependence of the superconducting gap $\Delta^{d+id'}$, we generalize our mean-field calculations to allow for spatially varying superconducting gap $\Delta(i)$ (instead of the gap with an uniform magnitude). As shown in Fig. 1 (a), the magnitude of gap is enhanced at edges and stay at a constant value

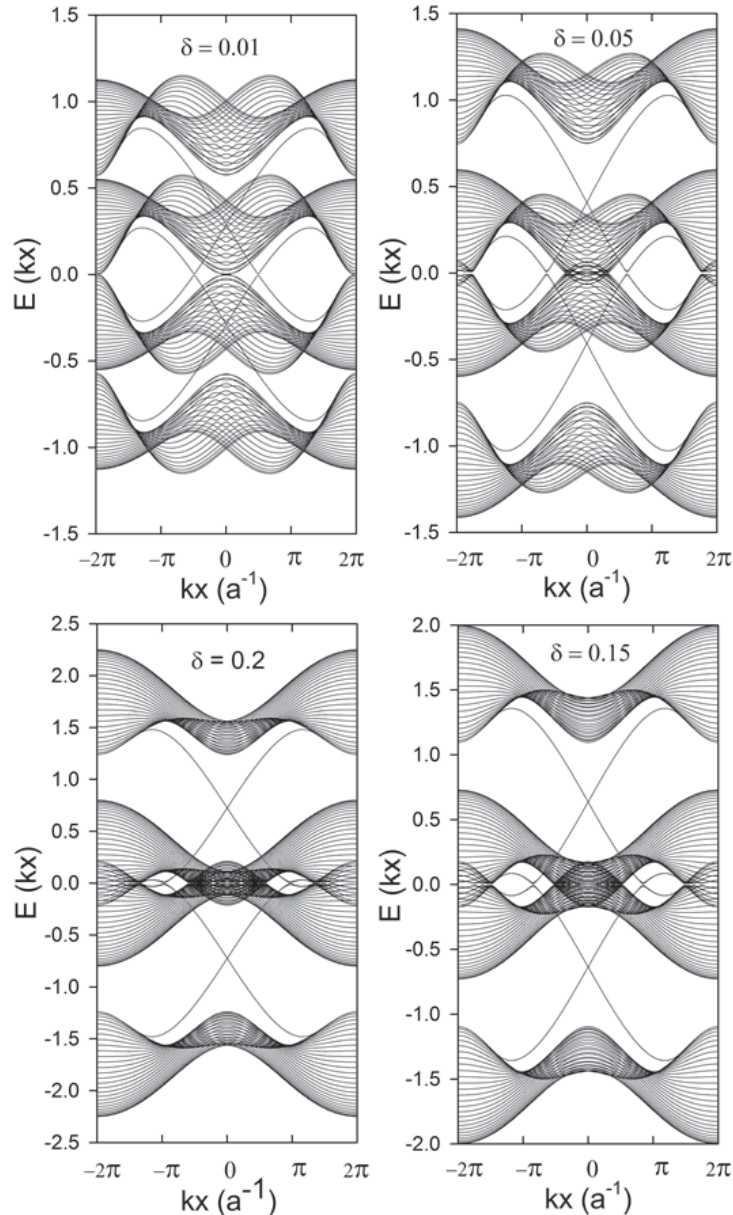


FIG. 2: Bogoliubov excitation spectrum of the Kane-Mele t-J model for different dopings. The parameters used here are: $J/t = 0.1$, $t_{SO}/t = 0.5$.

in the bulk. This can be understood as the electronic density of states (DOS) of the un-doped pure KM ribbon is enhanced at the edges due to the presence of the helical edge states. As a result, the superconducting pairing strength is enhanced at edges. However, the inhomogeneity of superconducting gap at the edges concerns only with the bulk states at a sizable negative energy. Since we focus in this work on the Majorana fermions near zero energy, far away from the superconducting states at edges, we therefore ignore this spatial inhomogeneity and consider only the superconducting gap with an uniform magnitude within our RMFT approach.

B. Doping evolution of the Bogoliubov excitation spectrum

Here, we provide the doping evolution of the Bogoliubov excitation spectrum as shown in Fig. 2. The spin-Chern phase with helical Majorana modes survive at low dopings. For $J/t = 0.1$, $t_{SO}/t = 0.5$, it survives for $0 < \delta < 0.2$. Above $\delta = 0.2$, the superconducting gap vanishes and the system is in the normal state. On the other hand, the chiral phase will prevail in the opposite regime $t_{SO} \ll \Delta_0$ for low dopings. However, the chiral superconductivity has been addressed extensively

(see Refs. 29, 35 in the main text). We will leave this issue out of the focus of our present work.

III. Z_2 TOPOLOGICAL INVARIANT

In this section, we provide details on obtaining the Z_2 topological number (or the spin Chern number) in the doped Kane-Mele t-J model following the approach in Ref. 2. First, the TKNN number, a topological (Chern) number, for the n -th band is defined as¹:

$$C_n = \frac{1}{2\pi i} \int_{BZ} dk^2 \nabla_{\mathbf{k}} \times \mathbf{A}(\mathbf{k}), \quad (\text{III.1})$$

where $\mathbf{A}(\mathbf{k}) \equiv \langle n(\mathbf{k}) | \nabla_{\mathbf{k}} | n(\mathbf{k}) \rangle$, $|n(\mathbf{k})\rangle$ is the Bloch state in the n -th band up to a normalization coefficient, which satisfies the Schroedinger equation $H(\mathbf{k})|n(\mathbf{k})\rangle = E_n(\mathbf{k})|n(\mathbf{k})\rangle$. The existence of $\mathbf{A}(\mathbf{k})$ implies that there is a non-trivial magnetic field across the first Brillouin Zone (FBZ). The FBZ of the honeycomb lattice we choose for the integration Eq. (III.1) is illustrated in Fig. 3, the parallelogram (area enclosed by red lines) spanned by vectors \mathbf{q}_1 and \mathbf{q}_2 in momentum space.

In order to numerically calculate the TKNN number covered by the entire FBZ (area enclosed by the solid red lines) in Fig. 3, we first discretize it into $N - 1 \times N - 1$ small flakes of parallelograms such as the smaller parallelogram $abcd$ (enclosed by solid black lines) in Fig. 3. The position of a discretized lattice point (that is the vertices of the small parallelograms) can be specified by a vector $\mathbf{k}_{i,j} = (k_{i1}, k_{j2})$, for $(i, j) \in [1, N]$ with its components

$$k_{i1} = \frac{1}{N-1} [(i-1) \times q_{1x} + (j-1) \times q_{2x}] ; \quad (\text{III.2})$$

$$k_{j2} = \frac{1}{N-1} [(i-1) \times q_{1y} + (j-1) \times q_{2y}], \quad (\text{III.3})$$

where q_{ix} and q_{iy} are the components of the vectors \mathbf{q}_1 and \mathbf{q}_2 with unit lattice spacing $|\bar{\mathbf{a}}| = 1$, they are given by

$$\mathbf{q}_1 = (q_{1x}, q_{1y}) = \left(\frac{4\pi}{3}, 0 \right) ; \quad (\text{III.4})$$

$$\mathbf{q}_2 = (q_{2x}, q_{2y}) = \left(\frac{2\pi}{3}, \frac{2\sqrt{3}\pi}{3} \right). \quad (\text{III.5})$$

The phase difference $\Delta\theta_1(\mathbf{k}_{ij})$ of $\Psi_n(\mathbf{k}) \equiv \langle \mathbf{k} | n(\mathbf{k}) \rangle$ travelling from a lattice point $\mathbf{k}_{i,j}$ to $\mathbf{k}_{i+1,j}$ can be computed to be

$$\begin{aligned} \Delta\theta_1(\mathbf{k}_{ij}) &= -i \ln \left[\frac{\Psi_n^\dagger(\mathbf{k}_{i,j}) \Psi_n(\mathbf{k}_{i+1,j})}{|\Psi_n^\dagger(\mathbf{k}_{i,j}) \Psi_n(\mathbf{k}_{i+1,j})|} \right]. \quad (\text{III.6}) \\ &\equiv -i \ln U_1(\mathbf{k}_{ij}), \end{aligned}$$

where

$$U_1(\mathbf{k}_{i,j}) \equiv \frac{\Psi_n^\dagger(\mathbf{k}_{i,j}) \Psi_n(\mathbf{k}_{i+1,j})}{|\Psi_n^\dagger(\mathbf{k}_{i,j}) \Psi_n(\mathbf{k}_{i+1,j})|} \quad (\text{III.7})$$

The subscript "1" of $\Delta\theta_1$ and $U_1(\mathbf{k}_{ij})$ represents that Ψ_n travels along the direction of \mathbf{q}_1 . Sum over $\Delta\theta$ of the four sides of the small parallelogram $abcd$ in Fig. 3 can one obtain the total phase shift of the Bloch wavefunction on the n -th band after circling around that small parallelogram. Compare with Eq. (III.1), we define the lattice $U(1)$ gauge field strength F_{ij}^n by

$$F_{ij}^n \equiv \ln U_1(\mathbf{k}_{i,j}) U_2(\mathbf{k}_{i+1,j}) U_1^{-1}(\mathbf{k}_{i,j+1}) U_2^{-1}(\mathbf{k}_{i,j}) \quad (\text{III.8})$$

Finally, we can calculate the TKNN number on the lattice associated the n -th band by

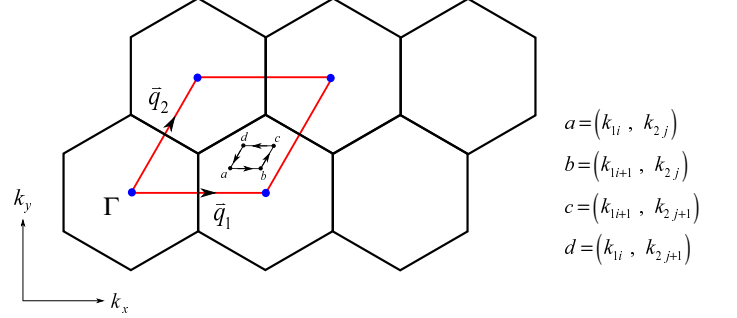


FIG. 3: The parallelogram enclosed by red solid lines is the area of entire FBZ with $\Gamma = (k_x = 0, k_y = 0)$. The small flake of parallelogram $abcd$ is the smallest unit after discretizing the FBZ for numerical calculation.

$$C_n = \frac{1}{2\pi i} \sum_{i,j} F_{ij}^n. \quad (\text{III.9})$$

For the same band we can further define a topological number, so-called the spin Chern number, as:

$$N_W = \frac{C_n - C_{\bar{n}}}{2}, \quad (\text{III.10})$$

where $C_{\bar{n}}$ is the TKNN number of the other degenerate eigenvector of the same band. Numerically, we obtain $C_{\bar{n}} = -C_n$, thus N_W is either 1 or -1 . We checked numerically that for the parameters used in Fig. 3 of the main text $|N_W|$ approaches to 1.

In the other extreme limit, $\Delta \gg t_{SO}$, we found that $N_{TKNN} \equiv C_n + C_{\bar{n}} = \pm 2$, and $N_W = 0$, as expected for $d + id'$ superconductivity in doped graphene³. Further studies suggest the existence of a quantum phase transition at a critical ratio of Δ/t_{SO} separating the spin-Chern phase with $N_W = \pm 1$ from the chiral (TKNN) phase with $N_{TKNN} = \pm 2$ (see Ref. 3).

IV. EFFECTIVE TRS SUPERCONDUCTIVITY NEAR THE DIRAC POINTS

In this section, we derive the low-energy effective TRS superconducting pairing of our model near Dirac points.

We re-express the $d + id'$ superconducting order parameter in terms of the electron operators $\psi_{\pm,k}$ which diagonalizes the tight-binding KM Hamiltonian with the corresponding eigenvalue $E^{\pm} = \pm(\sqrt{\epsilon_k^2 + \gamma_k^2} - \mu)$ (see Ref. 5):

$$\begin{pmatrix} c_{A,k}^{\uparrow} \\ c_{B,k}^{\uparrow} \end{pmatrix} = \begin{pmatrix} -\alpha_k^- & -\alpha_k^+ \\ \beta_k^- & \beta_k^+ \end{pmatrix} \begin{pmatrix} \psi_{+,k}^{\uparrow} \\ \psi_{-,k}^{\uparrow} \end{pmatrix} \quad (\text{IV.1})$$

and

$$\begin{pmatrix} c_{A,k}^{\downarrow} \\ c_{B,k}^{\downarrow} \end{pmatrix} = \begin{pmatrix} \alpha_k^+ & \alpha_k^- \\ \beta_k^+ & \beta_k^- \end{pmatrix} \begin{pmatrix} \psi_{+,k}^{\downarrow} \\ \psi_{-,k}^{\downarrow} \end{pmatrix} \quad (\text{IV.2})$$

where $\alpha_k^{\pm} = \beta^{\pm} \times \frac{\epsilon_k(\gamma_k \pm \sqrt{\epsilon_k^2 + \gamma_k^2})}{|\epsilon_k|^2}$, $\beta^{\pm} = \frac{|\epsilon_k|}{\sqrt{|\epsilon_k|^2 + (\gamma_k \pm \sqrt{\epsilon_k^2 + \gamma_k^2})^2}}$, and $(\alpha_k^{\pm})^* = -\alpha_{-k}^{\mp}$, $\beta^{\pm} = |\alpha_k^{\mp}|$. The $d + id'$ superconducting pairing term can be re-written as:

$$\begin{aligned} H_{\Delta} &= \sum_k \Delta_k^{d+id'} (c_{A,k}^{\uparrow} c_{B,k}^{\downarrow} - c_{A,k}^{\downarrow} c_{B,k}^{\uparrow}) + h.c. \\ &= \sum_k [\Delta_k^{--} \psi_{-,k}^{\uparrow} \psi_{-,k}^{\downarrow} + \Delta_k^{++} \psi_{+,k}^{\uparrow} \psi_{+,k}^{\downarrow} \\ &\quad + \Delta_k^{+-} \psi_{+,k}^{\uparrow} \psi_{-,k}^{\downarrow} + \Delta_k^{-+} \psi_{-,k}^{\uparrow} \psi_{+,k}^{\downarrow}] + h.c., \\ \Delta_k^{++(--) } &= |\alpha_k^{+(-)}| |\alpha_k^{-(+)}| \\ &\quad \times [\Delta_k^{d+id'} e^{i\theta(\alpha_k^{+(-)})} + \Delta_{-k}^{d+id'} e^{-i\theta(\alpha_k^{+(-)})}], \\ \Delta_k^{+-(-+)} &= \pm |\alpha_k^{+(-)}|^2 e^{i\theta(\alpha_k^{+(-)})} [\Delta_k^{d+id'} - \Delta_{-k}^{d+id'}], \end{aligned} \quad (\text{IV.3})$$

where $\alpha_k^{\pm} = |\alpha_k^{\pm}| e^{i\theta(\alpha_k^{\pm})}$ with $\theta(\alpha_k^{\pm})$ being the phase of α_k^{\pm} . In the presence of a finite SO coupling and hole-doping, the intra-band pairing of the lower band $\psi_{-,k}^{\uparrow} \psi_{-,k}^{\downarrow}$ with pairing gap function Δ_k^{--} dominates. The gap function $\Delta_{q_{\pm}}^{--}$ near Dirac points $K_{\pm} = (\frac{2\pi}{3\sqrt{3}}, \pm \frac{2\pi}{3})$ with $q_{\pm} = K_{\pm} + (\pm q_x, q_y)$ behaves to leading order in $|q|$ as an effective spin-singlet $p_x \pm ip_y$ -like superconductivity:

$$\Delta_{q_{\pm}}^{--} \sim -a_0 \Delta_0 i(q_x \mp iq_y) \quad (\text{IV.4})$$

with $a_0 = \frac{3te^{i\pi/3}}{12\sqrt{3}t_{SO}}$. Hence, our system behaves as an effective TRITOPs. In deriving Eq. (IV.4), we have used the following results:

$$\begin{aligned} \epsilon_{q_{\pm}} &\approx \pm \frac{3t}{2}(q_y + iq_x), \\ \alpha_{q_{-}}^{-} &\approx -\frac{\epsilon_{q_{-}}}{2\sqrt{3}t_{SO}}, \\ \alpha_{q_{-}}^{+} &\approx \epsilon_{q_{-}}/|\epsilon_{q_{-}}|. \end{aligned} \quad (\text{IV.5})$$

We have also used the approximated forms of $d + id'$ pairing gap $\Delta^{d+id'}(q)_{\pm}$ near the Dirac points, shown to be effectively a mixture of s -wave like (near K_{+}) and $p_x + ip_y$ -wave like (near K_{-}) superconducting pairing⁴:

$$\begin{aligned} \Delta^{d+id'}(q_{+}) &\approx 3\Delta_0 e^{i4\pi/3}, \\ \Delta^{d+id'}(q_{-}) &\approx \frac{3}{2}\Delta_0 e^{i\pi/3}(q_y - iq_x). \end{aligned} \quad (\text{IV.6})$$

¹ X.L. Qi, S.C. Zhang, Rev. Mod. Phys. **83**, 1057 (2011).

² Takahiro F Ukui, Yasuhiro H Atsugai and Hiroshi S Uzuki, J. Phys. Soc. Jpn. **74**, 6 (2005).

³ Shin-Ming Huang, Chung-Yu Mou and Chung-Hou Chung, (in preparation).

⁴ Yongjin Jiang, Dao-Xin Yao, Erica W. Carlson, Han-Dong Chen, and JiangPing Hu, Phys. Rev. B **77**, 235420 (2008).

⁵ W. Wu, M.M. Scherer, C. Honerkamp, K. Le Hur, Phys. Rev. B **87**, 094521 (2013).